Carbohydrate Polymers 87 (2012) 1249–1256

Contents lists available at SciVerse ScienceDirect

Carbohydrate Polymers

journal homepage: www.elsevier.com/locate/carbpol

Characterization of cellulose acetate-reinforced aliphatic–aromatic copolyester composites

Chin-San Wu*

Department of Chemical and Biochemical Engineering, Kao Yuan University, Kaohsiung County 82101, Taiwan, ROC

ARTICLE INFO

Article history:
Received 6 July 2011
Received in revised form 16 August 2011
Accepted 3 September 2011
Available online 10 September 2011

Keywords:
Poly(butylene adipate-*co*-terephthalate)
Cellulose acetate
Composites
Biodegradability

ABSTRACT

The biodegradability, morphology, mechanical, and thermal properties of composite materials composed of maleic anhydride-grafted poly(butylene adipate-*co*-terephthalate) (PBAT) and cellulose acetate (CA) were evaluated. Composites containing maleic anhydride-grafted PBAT (PBAT-g-MA/CA) exhibited noticeably superior mechanical properties due to greater compatibility between the two components. The dispersion of CA in the PBAT-g-MA matrix was highly homogeneous as a result of ester formation, and the consequent creation of branched and cross-linked macromolecules between the anhydride carboxyl groups of PBAT-g-MA and hydroxyl groups in CA. Each composite was buried in soil and monitored to assess biodegradability. Both the PBAT and the PBAT-g-MA/CA composite films were eventually completely degraded, and severe disruption of film structure was observed after 60–100 days of incubation. Although the degree of weight loss after burial indicated that both materials were biodegradable, even with high levels of CA, the higher water resistance of PBAT-g-MA/CA films indicated that they were more biodegradable than those made of PBAT.

1. Introduction

A great push is currently ongoing to develop biodegradable polyesters for use in applications including waste management and carbon emissions (Davis & Song, 2006; Kijchavengkul et al., 2010). Some polyesters exhibit similar water resistance properties as synthetic polymers and the biodegradability and biocompatibility of agricultural-based raw materials. For decades, research on biodegradable polymers has been focused on the development of plastic composites. More recently, these studies are being extended to address domestic waste. Both academic and industrial interests are focused on the utilization of biodegradable polyesters from renewable and/or fossil sources (Raquez, Deléglise, Lacrampe, & Krawczak, 2010; Satyanarayana, Arizaga, & Wypych, 2009).

The high cost and poor mechanical properties of aliphatic polyesters, however, have limited the realistic applications of these materials. Although aromatic polyesters have excellent mechanical properties and are relatively inexpensive, they do not biodegrade in most natural environments. Many researchers have synthesized aliphatic-*co*-aromatic copolyesters (Kambe, Ichihashi, Matsuzoe, Kato, & Shintani, 2009; Ki & Park, 2001) to generate biodegradable polymers with satisfactory mechanical properties. Poly(butylenes adipate-*co*-terephthalate)s (PBAT, Ecoflex®) are a commercialized aliphatic–aromatic, biodegradable copolymer available from BASF. Their mechanical and biodegradable properties were presented by Kumar and coauthors (Jiang, Wolcott, & Zhang, 2006; Kumar, Mohanty, Nayak, & Parvaiz, 2010; Madera-Santana, Misra, Drzal, Robledo, & Freile-Pelegrin, 2009). An optimal balance between biodegradability and physical properties (Shi, Ito, & Kikutani, 2005) is attained with aliphatic–aromatic copolyesters composed of 35–55 mol% aromatic units. PBAT has been used in composites with other polymers as a packaging material and has been proposed for use in agricultural applications including plastic bags, greenhouse films, and mulch films (Avérous & Digabel, 2006; Kijchavengkul et al., 2010). It is ideal for disposable packaging as it decomposes in compost within a few weeks or in soil without leaving any residue (Kijchavengkul, Auras, Rubino, Ngouajio, & Fernandez, 2008). As with other aliphatic polyesters, the biocompatibility of PBAT and its copolymers has led to several commercially successful applications (Gu, Zhang, Ren, & Zhan, 2008; Jao et al., 2010).

However, PBAT is relatively expensive. One approach to reduce the cost of PBAT composites is to blend them with natural biomaterials. Additionally, a continuing need exists to investigate more environmentally, friendly and sustainable materials as industry, in general, attempts to lessen its dependence on petroleum-based fuels and products. Toward this end, natural cellulose fibers that can increase the tensile strength of composites have been used as

* Fax: +886 7 6077788.
E-mail address: t50008@cc.kyu.edu.tw

0144-8617/$ – see front matter © 2011 Elsevier Ltd. All rights reserved.
doi:10.1016/j.carbpol.2011.09.009

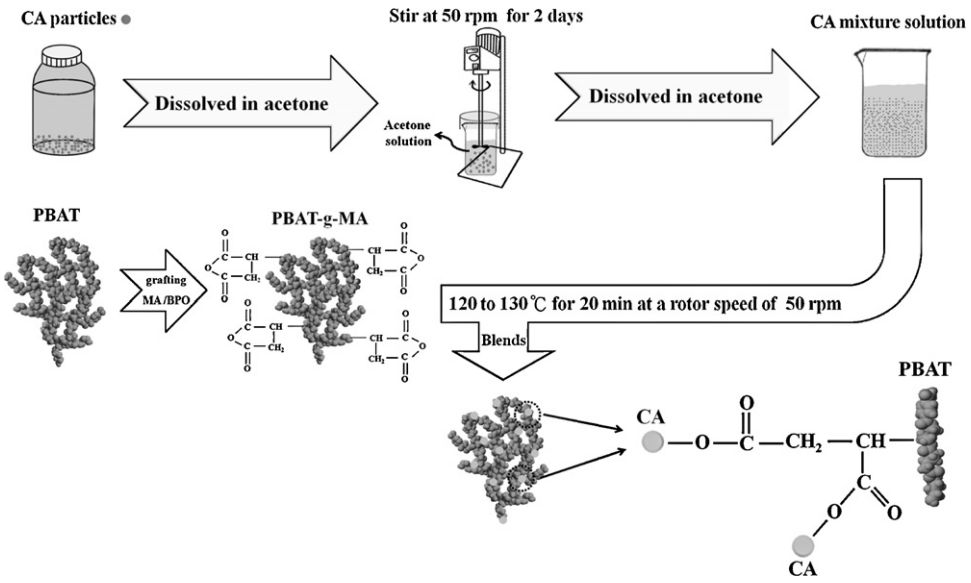

Scheme 1. Reaction scheme for the modification of PBAT and CA and the preparation of composite materials.

a means of reinforcing polymer matrices as a replacement for synthetic fibers. Cellulose acetate (CA) is an important and commonly used derivative of natural cellulose fibers (Edgar et al., 2001; Li & Frey, 2010).

Dried CA, which has been widely used in thermoplastic composites, can aggregate during solvent dispersion and needs a compatibilizing agent to wet the fibers (Kim, Lee, Choi, Kim, & Kim, 2007; Raquez, Nabar, Narayan, & Dubois, 2008a). However, the higher hydrophilicity of PBAT acts as a natural wetting agent in CA/PBAT composites. Composites of PBAT and CA therefore offer advantages in both biocompatibility and cost (Biswas, Saha, Lawton, Shogren, & Willett, 2006; Zhang & Hsieh, 2008). Furthermore, composites of biodegradable polymers and natural cellulose fibers have demonstrated complete biodegradation (Xu & Hanna, 2005) (Scheme 1).

This report describes the systematic investigation of the mechanical properties and biodegradability of CA composites with PBAT and maleic anhydride (MA)-grafted PBAT (PBAT-g-MA). The composites were characterized using Fourier-transform infrared spectroscopy (FTIR) and ^{13}C nuclear magnetic resonance (NMR) to identify bulk structural changes induced by the maleic anhydride moiety. Additionally, the effects of CA content on biodegradability were assessed for both types of composite. Composites developed in the current study were assessed as "green materials" via biodegradation studies in a soil environment.

2. Experimental

2.1. Materials

PBAT resins were purchased from BASF Corporation (Florham Park, NJ). Maleic anhydride (MA), obtained from Sigma (St. Louis, MO, USA), was purified before use by recrystallization from chloroform. Benzoyl peroxide (BPO; Sigma) was used as an initiator and was purified by dissolution in chloroform and reprecipitation in methanol. Cellulose acetate (3.5 g, degree of deacetylation 55%), supplied by Showa Chemical Co. Ltd. (Tokyo, Japan), was dissolved in 31.5 g of acetone to increase its dispersion in the polymer matrix and avoid aggregation.

2.2. Grafting reaction and sample preparation

Various reaction conditions including BPO and MA concentrations, reaction time and reaction temperature have been tested to screen for the optimal one. Thereafter, the grafting reaction was carried out with the optimal conditions as follows. Maleic anhydride was grafted onto PBAT dissolved in tetrahydrofuran in a nitrogen atmosphere at 45 °C; the polymerization reaction was initiated with 0.3 wt.% BPO. The reaction system was stirred at 60 rpm for 10 h. The grafted product (4 g) was then dissolved in 200 mL of refluxing tetrahydrofuran at 45 °C and the hot solution was filtered through several layers of cheesecloth. The cheesecloth was washed with 600 mL of acetone to remove the tetrahydrofuran-insoluble, unreacted maleic anhydride, and the remaining product was dried in a vacuum oven at 80 °C for 24 h. The tetrahydrofuran-soluble component of the filtrate was extracted five times using 600 mL of cold acetone for each extraction.

2.3. Determination of grafting percentage

Maleic anhydride loading of the tetrahydrofuran-soluble polymer (expressed as grafting percentage) was calculated from the acid number and was determined as follows. Firstly, about 2 g of copolymer was heated in 200 mL of refluxing tetrahydrofuran for 2 h. The hot solution was then titrated immediately with a 0.03 N ethanolic KOH solution, which was standardized against a solution of potassium hydrogen phthalate, with phenolphthalein used as an indicator. The acid number was calculated using Eq. (1) below, and the grafting percentage calculated using Eq. (2) (Grigoryeva & Kocsis, 2000):

$$\text{Acid number}\,(\text{mg KOH/g}) = \frac{V_{\text{KOH}}\,(\text{mL}) \times C_{\text{KOH}}\,(\text{N}) \times 56.1}{\text{polymer}\,(\text{N})} \quad (1)$$

$$\text{Grafting percentage}\,(\%) = \frac{\text{Acid number} \times 98.1}{2 \times 561} \times 100\% \quad (2)$$

A grafting percentage of approximately 1.12 wt.% when BPO loading was maintained at 0.3 wt.% and MA loading was maintained at 10 wt.%.

2.4. Composite preparation

Prior to composite fabrication, CA samples were cleaned with acetone and dried in an oven at 105 °C for 24 h. Composites were prepared in a "Plastograph" 200-Nm Mixer W50EHT with a blade rotor (Brabender, Dayton, OH). The composites were mixed between 120 and 130 °C for 25 min at a rotor speed of 50 rpm. Samples were prepared with mass ratios of CA to PBAT or to PBAT-g-MA of 5/95, 10/90, 15/85, and 20/80. Residual MA in the PBAT-g-MA reaction mixture was removed via acetone extraction prior to the preparation of PBAT-g-MA/CA. After mixing, the composites were pressed into thin plates with a hot press and placed in a dryer for cooling. These thin plates were cut to standard sample dimensions for further characterization.

2.5. NMR/FTIR XRD/TGA analyses

Solid-state ^{13}C NMR spectra were acquired with an AMX-400 NMR spectrometer at 100 MHz under cross-polarization while spinning at the magic angle. Power decoupling conditions were set with a 90° pulse and a 4-s cycle time. Infrared spectra of the samples were obtained using an FTS-7PC FTIR spectrophotometer (Bio-Rad, Hercules, CA). XRD diffractograms were recorded using a D/max 3-V X-ray diffractometer (Rigaku, Tokyo, Japan) with a Cu target and K_α radiation at a scanning rate of 2°/min. Thermogravimetry analysis (TA Instrument 2010 TGA, New Castle, DE) was used to assess whether two organic phase interactions influenced thermal stability degradation of hybrids. Samples were placed in alumina crucibles and tested with a thermal ramp over the temperature range of 30–600 °C at a heating rate of 10 °C/min and then the initial decomposition temperatures (IDT) of hybrids were obtained.

2.6. Mechanical testing

A mechanical tester (model LLOYD, LR5K type; Instron, Norwood, MA) was used to measure the tensile strength and the elongation at break, in accordance with ASTM D638. Test samples were prepared in a hydraulic press at 130 °C and conditioned at 50 ± 5% relative humidity for 24 h before making measurements. Measurements were made using a crosshead speed of 20 mm/min. Five measurements were performed for each sample and the results were averaged to obtain a mean value.

2.7. Composite morphology

A thin film of each composite was created with a hydraulic press and treated with hot water at 80 °C for 24 h before being coated with gold. The surface morphology of these thin films was observed using a scanning electron microscope (SEM, model S-1400; Hitachi, Tokyo, Japan).

2.8. Water absorption

Samples were prepared for water absorption measurements by cutting into 75 mm × 25 mm strips (150 ± 5 μm thick) in accordance with ASTM D570-81. The samples were dried in a vacuum oven at 50 ± 2 °C for 8 h, cooled in a desiccator, and then immediately weighed to the nearest 0.001 g (designated W_c). Thereafter, the samples were immersed in distilled water and maintained at 25 ± 2 °C for a 6-week period. During this time, they were removed from the water at 3-day intervals, gently blotted with tissue paper to remove excess water from their surfaces, immediately weighed to the nearest 0.001 g (designated W_w), and returned to the water. Each W_w value was an average value obtained from three measurements. The percentage of weight increase due to water absorption (W_f) was calculated to the nearest 0.01% according to Eq. (3):

$$\%W_f = \frac{W_w - W_c}{W_c} \times 100\% \quad (3)$$

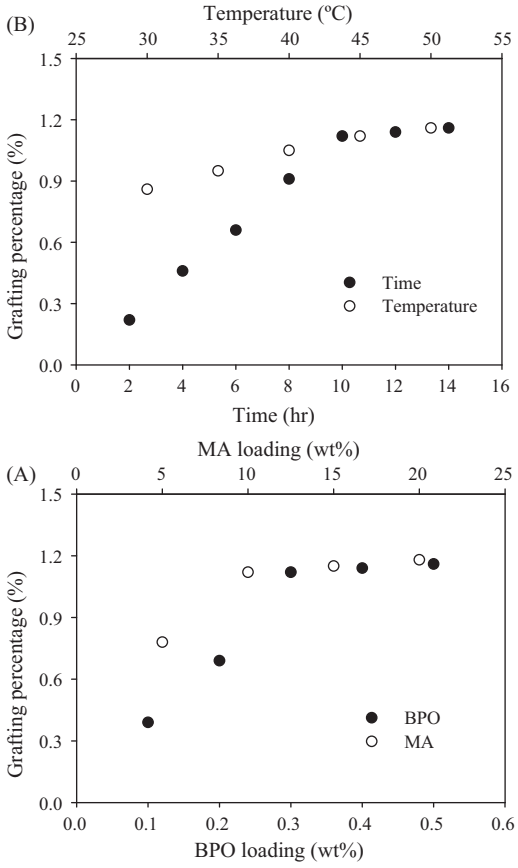

Fig. 1. (A) Effect of BPO and maleic anhydride loading on the grafting percentage of PBAT at 45 °C for 10 h. (B) Effect of reaction time and temperature on the grafting percentage of PBAT at 0.3 wt.% BPO for 10 wt.% MA.

2.9. Biodegradation studies

Biodegradability of the samples was assessed by measuring the weight loss of the composites over time in a soil environment. Samples measuring 35 mm × 20 mm × 1 mm were weighed and buried in boxes of alluvial-type soil that had been obtained in May 2010 from farmland topsoil before planting. The soil was sifted to remove large clumps and plant debris. Procedures for soil burial were as described by Tserki, Matzinos, Pavlidou, Vachliotis, and Panayiotou (2006). Soil was maintained at approximately 35% moisture by weight, and the samples were buried at a depth of 10–15 cm. A control box consisted of only samples and no soil. The buried samples were dug out after 15 days, washed in distilled water, dried in a vacuum oven at 50 ± 2 °C for 3 days, and equilibrated in desiccators for at least 1 day. The samples were then weighed before being returned to the soil.

3. Results and discussion

3.1. Effects of reaction conditions on percentage grafting for PBAT-g-MA

Fig. 1(A, solid symbols) shows the effect of BPO loading on grafting percentage of PBAT with maleic anhydride loading maintained at 10 wt.%. It was found that grafting percentage increased steadily

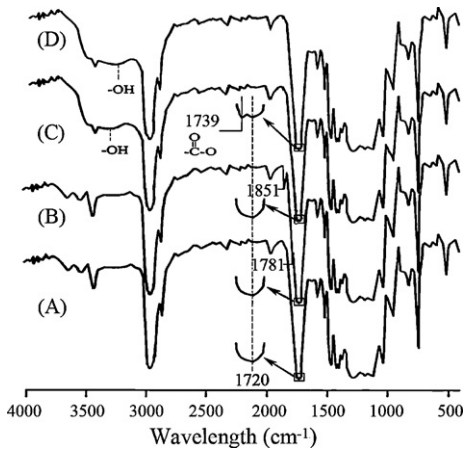

Fig. 2. FTIR spectra for (A) PBAT, (B) PBAT-g-MA, (C) PBAT/CA (10 wt.%), and (D) PBAT-g-MA/CA (10 wt.%).

with the BPO loading until 0.3 wt.%, while at BPO loading above 0.3 wt.%, grafting percentage approximated to a maximum value. The above findings are similar to those of Gaylord, Mehta, Kumar, and Tazi (1989). Fig. 1(A, open symbols) also illustrates the effect of maleic anhydride loading on grafting percentage with BPO loading maintained at 0.3 wt.%. A noticeable increase in grafting percentage occurred as the loading was increased from 0 to 10 wt.% with only a slight increase thereafter. It is probable, therefore, that 10 wt.% represents the approximate point at which MA is replaced as the rate-limiting factor by availability of free radical sites on the PBAT backbone. Sathe, Rao, and Devi (1994) has similar results.

Additionally, Fig. 1(B, solid symbols) gives the variations in grafting percentage with reaction time. The reaction temperature was 45 °C. It could be found that the grafting percentage increase steadily while the reaction time is increased to 10 h then the reaction will approach equilibrium. Fig. 1(B, open symbols) also illustrates the effect of reaction temperature on grafting percentage with reaction time for 10 h. A noticeable increase in grafting percentage occurred as the temperature was increased from 30 to 45 °C, with only a slight increase thereafter. It is probably, therefore, that 45 °C represents the approximate equilibrium point. By the above results, the optimal reaction conditions for graft copolymerization of PBAT-g-MA were at 45 °C for 10 h when BPO loading was maintained at 0.3 wt.% and MA loading was maintained at 10 wt.%.

3.2. FTIR/NMR analysis

The FTIR spectra of unmodified PBAT and PBAT-g-MA are shown in Fig. 2A and B, respectively. The characteristic transitions of PBAT (Raquez, Nabar, Narayan, & Dubois, 2008b) at 3300–3700, 1700–1760, and 500–1500 cm^{-1} appeared in the spectra of both polymers, with two additional shoulders observed at 1781 and 1851 cm^{-1} in the modified PBAT spectrum. These features are characteristic of anhydride carboxyl groups. Similar results have been reported previously (Nakason, Kaesaman, & Supasanthitikul, 2004). The shoulders represent free acid in the modified polymer and therefore denote the grafting of MA onto PBAT.

In the composite PBAT/CA (10 wt.%), the peak assigned to the O–H stretching vibration at 3200–3700 cm^{-1} intensified (Fig. 2C) due to contributions from the –OH group of CA. The FTIR spectrum of the PBAT-g-MA/CA (10 wt.%) composite in Fig. 2(D) revealed a peak at 1739 cm^{-1} that was not present in the FTIR spectrum of the PBAT/CA (10 wt.%) blend. This peak was assigned to the ester carbonyl stretching vibration of the copolymer. Wu (2009) also reported an absorption peak at 1739 cm^{-1} for this ester carbonyl group. These data suggest the formation of branched and

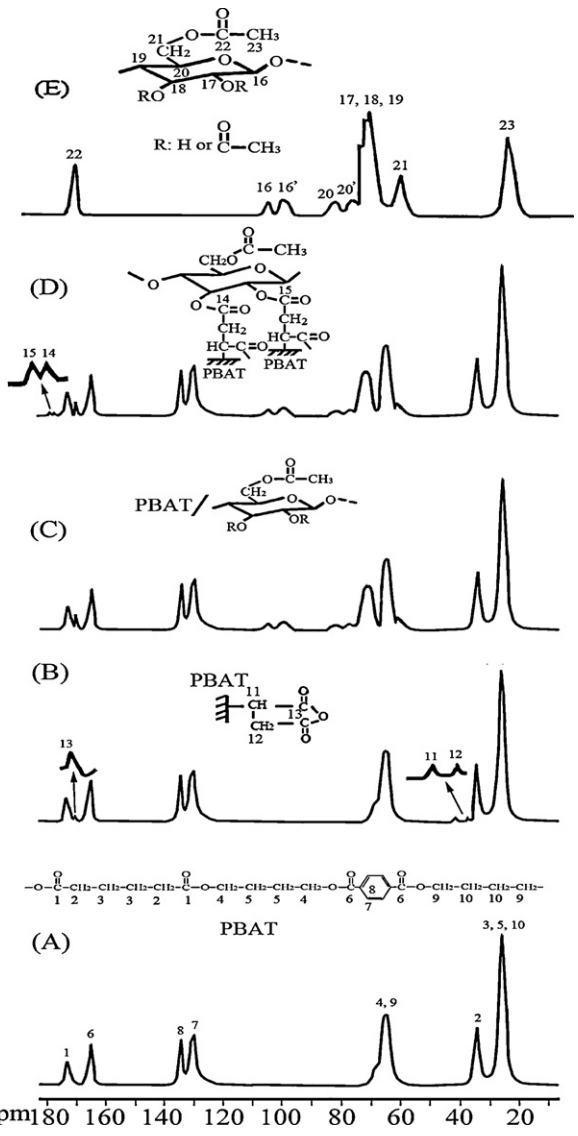

Fig. 3. Solid-state ^{13}C NMR spectra for (A) PBAT, (B) PBAT-g-MA, (C) PBAT/CA (10 wt.%), (D) PBAT-g-MA/CA (10 wt.%), and (E) CA.

cross-linked macromolecules in PBAT-g-MA/CA by covalent reaction of the anhydride carboxyl groups in PBAT-g-MA with the hydroxyl groups of CA.

To further confirm this conclusion, solid-state ^{13}C NMR spectra of PBAT and PBAT-g-MA were compared in Fig. 3(A and B), respectively. The ^{13}C NMR spectrum of neat PBAT (Fig. 3A) was similar to that measured by Herrera, Franco, Rodríguez-Galán, and Puiggalí (2002) and exhibited 10 peaks: (1) δ = 173.8 ppm; (2) δ = 34.5 ppm; (3), (5), (10) δ = 26.3 ppm; (4), (9) δ = 65.1 ppm; (6) δ = 164.8 ppm; (8) δ = 134.3 ppm; and (7) δ = 129.8 ppm. The ^{13}C NMR spectrum of PBAT-g-MA showed additional peaks (11: δ = 41.7 ppm; 12: δ = 37.7 ppm; 13: –C=O δ = 170.5 ppm), thus confirming that MA was covalently grafted onto PBAT.

The solid-state ^{13}C NMR spectra of PBAT-g-MA/CA (10 wt.%), PBAT/CA (10 wt.%), and CA are shown in Fig. 3(C–E). The CA spectra in Fig. 3(E) are similar to those reported by Xiao et al. (2004). Relative to unmodified PBAT, additional peaks were observed in the spectra of composites containing PBAT-g-MA. These additional peaks were located at δ = 41.7 ppm (11) and δ = 37.7 ppm (12). These same features were observed in previous studies (Marshall & Wilson, 1988; Wu, 2009) and indicate grafting of MA onto PBAT. However, the peak at δ = 170.5 ppm (C=O) (13) (shown in Fig. 3B),

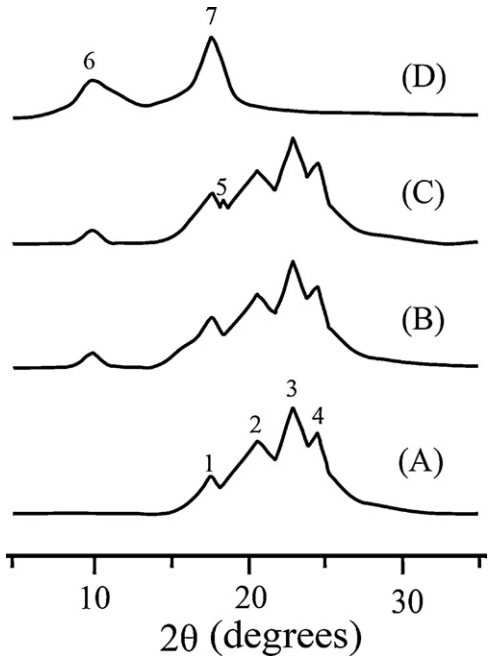

Fig. 4. X-ray diffractograms for (A) PBAT, (B) PBAT/CA (10 wt.%), (C) PBAT-g-MA/CA (10 wt.%), and (D) CA.

which is also typical for MA grafted onto PBAT, was absent in the solid-state spectrum of PBAT-g-MA/CA (10 wt.%). This is most likely a result of an additional condensation reaction between the anhydride carboxyl group of MA and the –OR group of CA that caused the peak at δ = 170.5 ppm to split into two bands (δ = 177.7 and 179.1 ppm). This additional reaction converted the fully acylated groups in the original CA to esters (represented by peaks 14 and 15 in Fig. 3C) and did not occur between PBAT and CA, as indicated by the absence of corresponding peaks in the FTIR spectrum of PBAT/CA (10 wt.%) in Fig. 3D. The formation of ester groups significantly affects the mechanical properties of PBAT-g-MA/CA and is discussed in greater detail in the following sections.

3.3. X-ray diffraction

X-ray diffractograms of pure PBAT, PBAT/CA (10 wt.%), PBAT-g-MA/CA (10 wt.%), and CA are shown in Fig. 4(A–D). Similar to the results of Chivrac, Kadlecova, Pollet, and Avérous (2006), pure PBAT (Fig. 4A) exhibited four diffraction peaks at about 17.5°, 20.5°, 22.9°, and 24.5°, designated 1, 2, 3, and 4, respectively. The diffractogram of neat CA in Fig. 4(D) also revealed two peaks at 10.1° and 22.6°, designated 6 and 7, respectively (Filho, Silva, Meireles, Assuncao, & Otaguro, 2005). A comparison of the diffractograms of PBAT/CA and CA suggests that peaks 6 and 7 may be the result of physical dispersion of CA throughout the PBAT matrix. Furthermore, Fig. 4(C) shows an additional peak at 18.2° (designated 5) in the diffractogram of the PBAT-g-MA/CA composite. This peak, also identified by Danyadi et al. (2007), may have been caused by the formation of ester carbonyl groups. This would indicate that the crystalline structure of the PBAT/CA composite was altered when PBAT-g-MA was used in place of PBAT.

3.4. Thermal behavior

The thermal stability of the PBAT, PBAT-g-MA, CA and its composites is measured with TGA under nitrogen atmosphere, respectively. It is known that the defunctionalization of CA can be realized by thermal decomposition. In the present study, TGA was

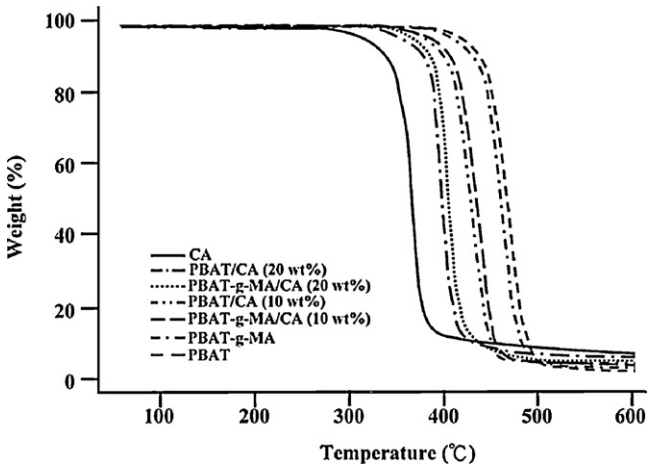

Fig. 5. Effect of CA content on TGA curves is shown for PBAT/CA and PBAT-g-MA/CA composites.

used to determine the effect of CA content on the weight loss of hybrids, and the results are presented in Fig. 5 and Table 1. For both composites, IDT decreased with increasing CA content. This may be due to CA-induced expansion of PBAT or PBAT-g-MA, which produces a slack polymer structure and a reduced IDT.

At the same CA content, the PBAT-g-MA/CA composites had a higher IDT than the PBAT/CA composites (Fig. 5 and Table 1). This reduced IDT was probably caused by increased difficulty in arranging the polymer chain, due to the already noted prohibition of movement of polymer segments by CA. Similarly, another potential cause is the condensation reaction, which leads to increased adhesion of CA with PBAT-g-MA. These results are similar to those obtained with composites of polymer and other natural fibers (Kim et al., 2007). This outcome is a result of the difference in interfacial forces in the two hybrids: the weaker hydrogen bonds of PBAT/CA compared with the stronger coordination sites associated with the anhydride carboxyl groups of PBAT-g-MA/CA. The values of thermal stability (IDT) in PBAT-g-MA/CA were approximately 4–12 °C higher than those of PBAT/CA. These higher IDT values were likely due to the formation of ester carbonyl groups as discussed above.

3.5. Composite morphology

In most composite materials, effective wetting and uniform dispersion of all components in a given matrix and strong interfacial adhesion between the phases are required to obtain a composite with satisfactory mechanical properties. In the current study, CA may be thought of as a dispersed phase within a PBAT or PBAT-g-MA matrix. To evaluate the composite morphology, SEM was used to examine tensile fractures in the surfaces of PBAT/CA (10 wt.%) and PBAT-g-AA/CA (10 wt.%) samples. The SEM microphotograph of PBAT/CA (10 wt.%) in Fig. 6(A) shows that the CA in this composite tended to agglomerate into bundles and was unevenly distributed in the matrix. This poor dispersion was due to the formation of hydrogen bonds among CA fibers and the disparate hydrophilicities

Table 1
Effect of CA content on the thermal properties of PBAT/CA and PBAT-g-MA/CA composites.

CA (wt.%)	PBAT/CA IDT (°C)	PBAT-g-MA/CA IDT (°C)
0	422	416
5	405	409
10	388	398
15	377	389
20	366	378

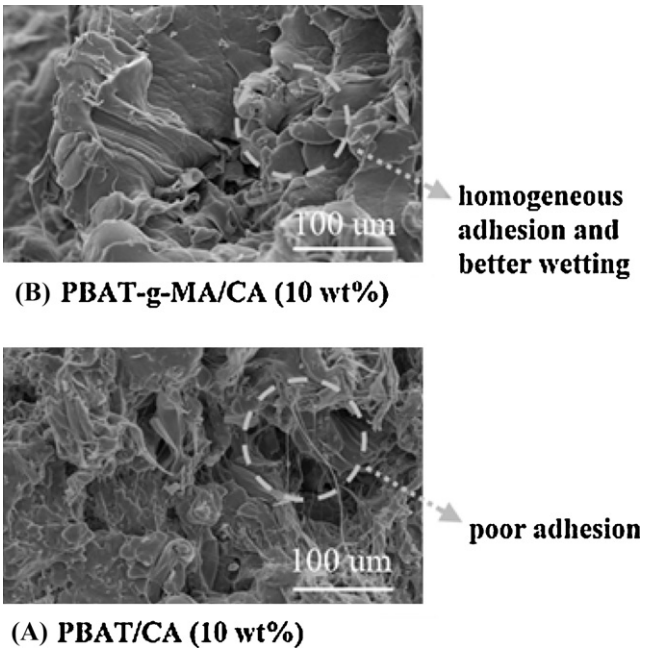

Fig. 6. SEM photomicrographs of the distribution and adhesion of CA in (A) PBAT/CA (10 wt.%) and (B) PBAT-g-MA/CA (10 wt.%) composites.

of PBAT and CA. Poor wetting was also observed in these composites (marked in Fig. 6A) due to large differences in surface energy between the CA and the PBAT matrix (Wong, Zahi, Low, & Lim, 2010). The PBAT-g-MA/CA (10 wt.%) photomicrograph in Fig. 6(B) shows more homogeneous dispersion and better wetting of CA in the PBAT-g-MA matrix, indicated by the complete coverage of PBAT-g-MA on the fiber and the removal of both materials when a fiber was pulled from the bulk. This improved interfacial adhesion was due to the similar hydrophilicity of the two components, which allowed for the formation of branched and cross-linked macromolecules, and the prevention of hydrogen bonding between CA.

3.6. Mechanical properties

Fig. 7 shows the variations in tensile strength and elongation at break as a function of CA content for PBAT/CA and PBAT-g-MA/CA composites. The tensile strength and elongation of pure PBAT decreased after grafting with maleic anhydride. For PBAT/CA composites (Fig. 7A), the tensile strength decreased markedly and continuously with increasing CA content, which was attributable to poor dispersion of CA in the PBAT matrix as previously discussed and shown in Fig. 6(A). The effect of this incompatibility on the mechanical properties of the composites was substantial. The PBAT-g-MA/CA composites in Fig. 7(A) exhibited a unique behavior in which the tensile strength at break increased with increasing CA content despite the lower tensile strength of PBAT-g-MA relative to that of pure PBAT. Furthermore, the tensile strength of PBAT-g-MA/CA composites was constant with greater than 10% CA. This behavior was likely due to enhanced dispersion of CA in the PBAT-g-MA matrix resulting from the formation of branched or cross-linked macromolecules.

Fig. 7(B) also indicates lower elongation at break values for the PBAT/CA composites relative to that of the PBAT-g-MA/CA composites. In PBAT/CA, the CA tended to agglomerate into bundles, illustrating the poor compatibility between the two phases. In the PBAT-g-MA/CA composites (Fig. 7B), the elongation at break also decreased with increasing amounts of CA but exhibited greater elongation values compared to the PBAT/CA composites. However, these values were still lower than those of pure PBAT. These results

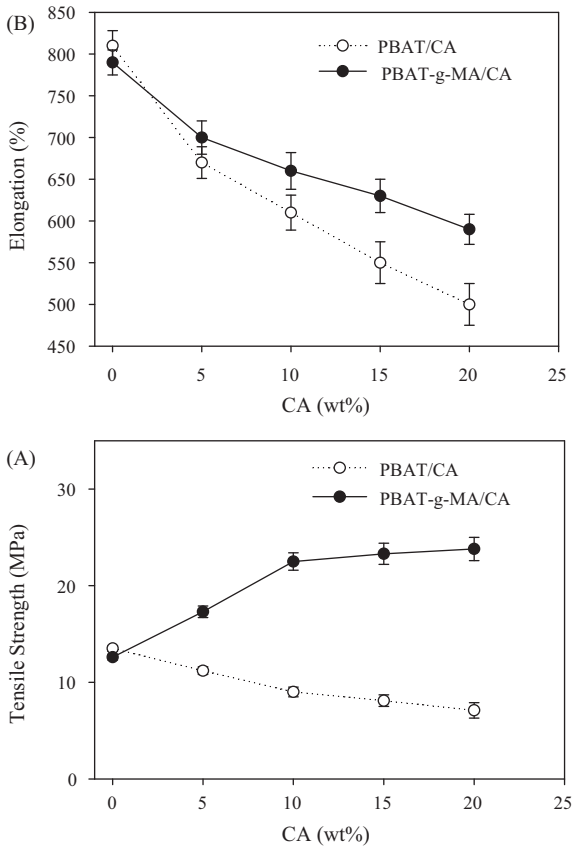

Fig. 7. The effect of CA content on (A) tensile strength and (B) elongation at break for PBAT/CA and PBAT-g-MA/CA composites.

are similar to those of Mishra, Naik, and Patil (2000). The data in Fig. 7 indicate that the grafting reaction in PBAT-g-MA/CA composites improved the tensile strength and elongation of PBAT/CA. However, the degree of enhancement in elongation was smaller than that in tensile strength.

3.7. Water absorption

At the same CA content, the PBAT-g-MA/CA composites exhibited a higher resistance to water absorption than the PBAT/CA

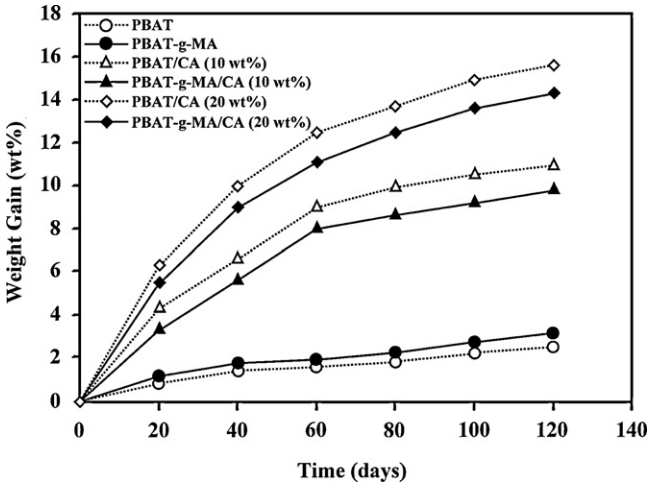

Fig. 8. Percent weight gain due to the absorption of water for PBAT/CA and PBAT-g-MA/CA composites.

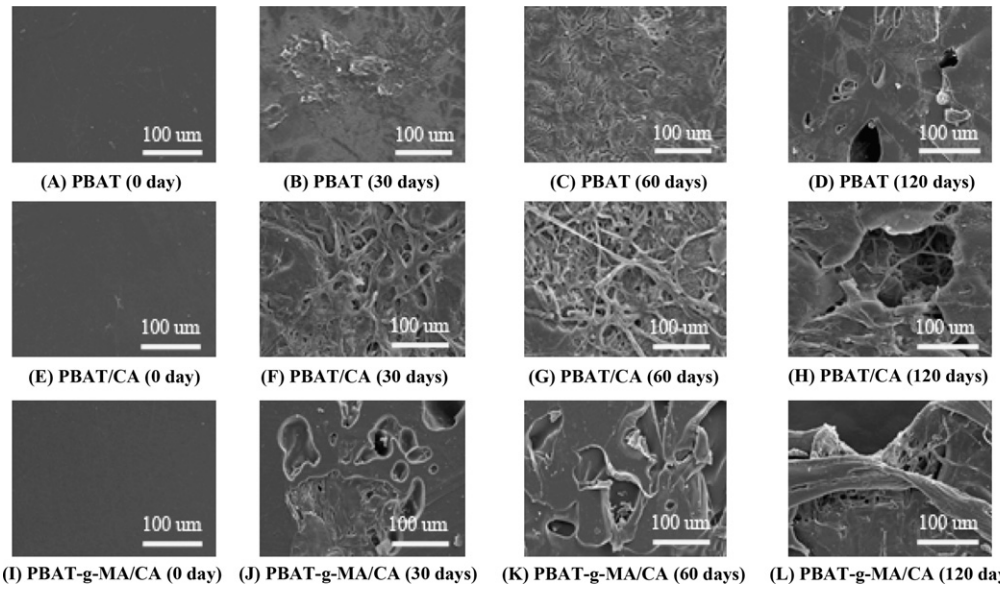

Fig. 9. SEM micrographs of the morphology of PBAT (A–D), PBAT/CA (E–H), and PBAT-g-MA/CA (I–L) films as a function of incubation time in soil.

composites (Fig. 8). The water resistance of the PBAT-g-MA/CA composites was moderate, and the interaction of MA-grafted PBAT with CA increased the hydrophobicity of CA in these composites. For both PBAT/CA and PBAT-g-MA/CA, the percent water gain over the 120-day test period increased with increasing CA content. Because the polymer chain arrangement in these systems is presumably random, the above result was likely due to decreased chain mobility with greater amounts of CA and to the hydrophilic character of CA, which adheres weakly to the more hydrophobic PBAT.

3.8. Biodegradation in soil

Changes in the morphology of the PBAT, PBAT/CA, and PBAT-g-MA/CA composites were noted as a function of the amount of time buried in soil. SEM photomicrographs taken after 30, 60, and 120 days illustrate the extent of morphological change (Fig. 9). PBAT/CA (10 wt.%; Fig. 9F–H) exhibited larger and deeper pits that appeared to be more randomly distributed relative to those in the PBAT-g-MA/CA (10 wt.%) composites (Fig. 9J–L). These analyses also indicate that biodegradation of the CA phase in PBAT/CA (10 wt.%) increased with time, confirming the results presented in Fig. 10.

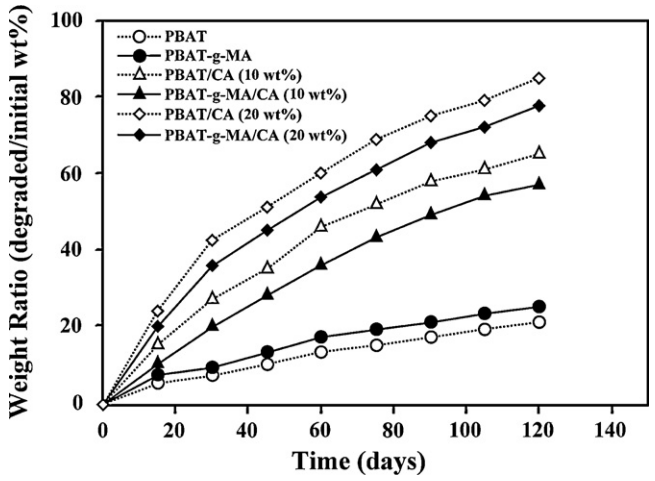

Fig. 10. Weight loss percentages of PBAT, PBAT-g-MA, PBAT/CA, and PBAT-g-MA/CA as a function of incubation time in soil.

After a 30-day incubation period, cell growth with gradual erosion and cracking was observed on the surface of the PBAT matrix (Fig. 9B). After 60 days, the disruption of the PBAT matrix became more obvious (Fig. 9C). This degradation was confirmed by the increasing weight loss of the PBAT matrix as a function of incubation time (Fig. 10), which reached nearly 20% after only 120 days. The most likely cause of this weight loss was biodegradation.

The SEM photomicrographs in Fig. 9 indicate that the PBAT-g-MA/CA (10 wt.%) composites were more readily degraded than neat PBAT. After a 30-day incubation period, the PBAT-g-MA/CA composite was coated with a biofilm of bacterial cells (Fig. 9J), indicating more cell growth than that observed on PBAT at the same incubation time. Moreover, at 60 and 120 days, larger pores were apparent in the PBAT-g-MA/CA composite (Fig. 9K and L), indicating a higher level of degradation. The rate of weight loss in the PBAT-g-MA/CA composites was also accelerated relative to that of PBAT, exceeding 10% after 120 days (Fig. 10). These results demonstrate that the addition of CA to the MA-grafted PBAT enhanced the biodegradability of the composite.

Fig. 10 shows the percent weight change as a function of time for PBAT/CA and PBAT-g-MA/CA composites buried in the soil compost. For both composites, the degree of weight loss increased with CA content. Composites with 10 wt.% CA degraded rapidly over the first 60 days, losing a mass equivalent to their approximate CA content, and showed a gradual decrease in weight over the next 60 days. PBAT-g-MA/CA exhibited a weight loss of approximately 3–11 wt.%.

4. Conclusions

The compatibility, thermal behavior and mechanical properties of CA blended with PBAT and maleic anhydride-modified PBAT (PBAT-g-MA) were examined. FTIR and NMR analyses revealed the formation of ester groups due to reactions between –OH groups in CA and anhydride carboxyl groups in PBAT-g-MA, which significantly altered the structure of the composite material. The morphology of PBAT-g-MA/CA composites was consistent with good adhesion between the CA phase and the PBAT-g-MA matrix. In mechanical tests, PBAT-g-MA enhanced the mechanical properties of the composite, especially the tensile strength. Although the water resistance of PBAT-g-MA/CA was higher than that of PBAT/CA, the biodegradation rate of PBAT-g-MA/CA was lower than that of PBAT/CA, but still higher than that of pure PBAT,

when incubated in soil. After 120 days, the PBAT-g-MA/CA (20 wt.%) composite suffered greater than 75% weight loss. The degree of biodegradation increased with increasing CA content.

References

Avérous, L. & Digabel, F. L. (2006). Properties of biocomposites based on lignocellulosic fillers. *Carbohydrate Polymers*, *66*(4), 480–493.

Biswas, A., Saha, B. C., Lawton, J. W., Shogren, R. L. & Willett, J. L. (2006). Process for obtaining cellulose acetate from agricultural by-products. *Carbohydrate Polymers*, *64*(1), 134–137.

Chivrac, F., Kadlecova, Z., Pollet, E. & Avérous, L. (2006). Aromatic copolyester-based nano-biocomposites: Elaboration, structural characterization and properties. *Journal of Polymers and the Environment*, *14*(4), 393–401.

Danyadi, L., Janecska, T., Szabo, Z., Nagy, G., Moczo, J. & Pukanszky, B. (2007). Wood flour filled PP composites: Compatibilization and adhesion. *Composites Science and Technology*, *67*(13), 2838–2846.

Davis, G. & Song, J. H. (2006). Biodegradable packaging based on raw materials from crops and their impact on waste management. *Industrial Crops and Products*, *23*(2), 147–161.

Edgar, K. J., Buchanan, C. M., Debenham, J. S., Rundquist, P. A., Seiler, B. D., Schelton, M. C., et al. (2001). Advances in cellulose ester performance and application. *Progress in Polymer Science*, *26*(9), 1605–1688.

Filho, G. R., Silva, R. C., Meireles, C. S., Assuncao, R. M. N. & Otaguro, H. (2005). Water flux through blends from waste materials: Cellulose acetate (from sugar cane bagasse) with polystyrene (from plastic cups). *Journal of Applied Polymer Science*, *96*(2), 516–522.

Gaylord, N. G., Mehta, R., Kumar, V. & Tazi, M. (1989). High density polyethylene-g-maleic anhydride preparation in presence of electron donors. *Journal of Applied Polymer Science*, *38*(2), 359–371.

Grigoryeva, O. P. & Kocsis, J. K. (2000). Melt grafting of maleic anhydride onto an ethylene-pylene-diene terpolymer (EPDM). *European Polymer Journal*, *36*(7), 1419–1429.

Gu, S. Y., Zhang, K., Ren, J. & Zhan, H. (2008). Melt rheology of polylactide/poly(butylenes adipate-co-terephthalate) blends. *Carbohydrate Polymers*, *74*(1), 79–85.

Herrera, R., Franco, L., Rodríguez-Galán, A. & Puiggalí, J. (2002). Characterization and degradation behavior of poly(butylene adipate-co-terephthalate)s. *Journal of Polymer Science: Part A: Polymer Chemistry*, *40*(23), 4141–4157.

Jao, W. C., Lin, C. H., Hsieh, J. Y., Yeh, Y. H., Liu, C. Y. & Yang, M. C. (2010). Effect of immobilization of polysaccharides on the biocompatibility of poly(butyleneadipate-co-terephthalate) films. *Polymer for Advanced Technologies*, *21*(8), 543–553.

Jiang, L., Wolcott, M. P. & Zhang, J. (2006). Study of biodegradable polylactide/poly(butylene adipate-co-terephthalate) blends. *Biomacromolecules*, *7*(1), 199–207.

Kambe, T. N., Ichihashi, F., Matsuzoe, R., Kato, S. & Shintani, N. (2009). Degradation of aliphatic–aromatic copolyesters by bacteria that can degrade aliphatic polyesters. *Polymer Degradation and Stability*, *94*(11), 1901–1905.

Ki, H. C. & Park, O. O. (2001). Synthesis, characterization and biodegradability of the biodegradable aliphatic–aromatic random copolyesters. *Polymer*, *42*(5), 1849–1861.

Kijchavengkul, T., Auras, R., Rubino, M., Ngouajio, M. & Fernandez, R. T. (2008). Assessment of aliphatic–aromatic copolyester biodegradable mulch films. Part I: Field study. *Chemosphere*, *71*(5), 942–953.

Kijchavengkul, T., Auras, R., Rubino, M., Alvarado, E., Montero, J. R. C. & Rosales, J. M. (2010). Atmospheric and soil degradation of aliphatic–aromatic polyester films. *Polymer Degradation and Stability*, *95*(2), 99–107.

Kim, H. S., Lee, B. H., Choi, S. W., Kim, S. & Kim, H. J. (2007). The effect of types of maleic anhydride-grafted polypropylene (MAPP) on the interfacial adhesion properties of bio-flour-filled polypropylene composites. *Composites: Part A: Applied Science and Manufacturing*, *38*(6), 1473–1482.

Kumar, M., Mohanty, S., Nayak, S. K. & Parvaiz, M. R. (2010). Effect of glycidyl methacrylate (GMA) on the thermal, mechanical and morphological property of biodegradable PLA/PBAT blend and its nanocomposites. *Bioresource Technology*, *101*(21), 8406–8415.

Li, L. & Frey, M. (2010). Preparation and characterization of cellulose nitrate–acetate mixed ester fibers. *Polymer*, *51*(16), 3774–3783.

Madera-Santana, T. J., Misra, M., Drzal, L. T., Robledo, D. & Freile-Pelegrin, Y. (2009). Preparation and characterization of biodegradable agar/poly(butylene adipate-co-terephatalate) composites. *Polymer Engineering and Science*, *49*(6), 1117–1126.

Marshall, G. L. & Wilson, S. J. (1988). The characterisation of styrene cross-linked polyester resins using swollen-state ^{13}C NMR spectroscopy. *European Polymer Journal*, *24*(10), 939–945.

Mishra, S., Naik, J. B. & Patil, Y. P. (2000). The compatibilising effect of maleic anhydride on swelling and mechanical properties of plant-fiber-reinforced novolac composites. *Composites Science and Technology*, *60*(9), 1729–1735.

Nakason, C., Kaesaman, A. & Supasanthitikul, P. (2004). The grafting of maleic anhydride onto natural rubber. *Polymer Testing*, *23*(1), 35–41.

Raquez, J. M., Deléglise, M., Lacrampe, M. F. & Krawczak, P. (2010). Thermosetting (bio)materials derived from renewable resources: A critical review. *Progress in Polymer Science*, *35*(4), 487–509.

Raquez, J. M., Nabar, Y., Narayan, R. & Dubois, P. (2008a). Novel high-performance talc/poly[(butylenes adipate)-co-terephthalate] hybrid materials. *Macromolecular Materials and Engineering*, *293*(4), 310–320.

Raquez, J. M., Nabar, Y., Narayan, R. & Dubois, P. (2008b). In situ compatibilization of maleated thermoplastic starch/polyester melt-blends by reactive extrusion. *Polymer Engineering and Science*, *48*(9), 1747–1754.

Sathe, S. N., Rao, G. S. S. & Devi, S. (1994). Grafting of maleic anhydride onto polypropylene: Synthesis and characterization. *Journal of Applied Polymer Science*, *53*(2), 239–245.

Satyanarayana, K. G., Arizaga, G. G. C. & Wypych, F. (2009). Biodegradable composites based on lignocellulosic fibers—An overview. *Progress in Polymer Science*, *34*(9), 982–1021.

Shi, X. Q., Ito, H. & Kikutani, T. (2005). Characterization on mixed-crystal structure and properties of poly(butylene adipate-co-terephthalate) biodegradable fibers. *Polymer*, *46*(25), 11442–11450.

Tserki, V., Matzinos, P., Pavlidou, E., Vachliotis, D. & Panayiotou, C. (2006). Biodegradable aliphatic polyesters. Part I. Properties and biodegradation of poly(butylene succinate-co-butylene adipate). *Polymer Degradation and Stability*, *91*(2), 367–376.

Wong, K. J., Zahi, S., Low, K. O. & Lim, C. C. (2010). Fracture characterisation of short bamboo fibre reinforced polyester composites. *Materials and Design*, *31*(9), 4147–4154.

Wu, C. S. (2009). Renewable resource-based composites of recycled natural fibers and maleated polylactide bioplastic: Characterization and biodegradability. *Polymer Degradation and Stability*, *94*(7), 1076–1084.

Xiao, D., Hu, J., Zhang, M., Li, M., Wang, G. & Yao, H. (2004). Synthesis and characterization of camphorsulfonyl acetate of cellulose. *Carbohydrate Research*, *339*(11), 1925–1931.

Xu, Y. & Hanna, M. A. (2005). Preparation and properties of biodegradable foams from starch acetate and poly(tetramethylene adipate-co-terephthalate). *Carbohydrate Polymers*, *59*(4), 521–529.

Zhang, L. & Hsieh, Y. L. (2008). Ultra-fine cellulose acetate/poly(ethylene oxide) bicomponent fibers. *Carbohydrate Polymers*, *71*(2), 196–207.